

Dynamo action at low magnetic Prandtl numbers: mean flow versus fully turbulent motions

Y Ponty¹, P D Mininni², J-F Pinton³, H Politano¹ and A Pouquet²

¹ CNRS UMR6202, Laboratoire Cassiopée, Observatoire de la Côte d'Azur, BP 4229, Nice Cedex 04, France

² NCAR, P O Box 3000, Boulder Colorado 80307-3000, USA

³ CNRS UMR5672, Laboratoire de Physique, École Normale Supérieure de Lyon, 46 Allée d'Italie, 69007 Lyon, France

E-mail: Yannick.PONTY@obs-nice.fr

New Journal of Physics **9** (2007) 296

Received 17 January 2007

Published 31 August 2007

Online at <http://www.njp.org/>

doi:10.1088/1367-2630/9/8/296

Abstract. We compute numerically the threshold for dynamo action in Taylor–Green (TG) swirling flows. Kinematic dynamo calculations, for which the flow field is fixed to its time average, are compared to dynamical runs, with the Navier–Stokes and induction equations jointly solved. The dynamo instability for the kinematic calculations is found to have two branches. The dynamical dynamo threshold at low Reynolds numbers lies within the low branch, while at high Reynolds numbers it gets closer to the high branch. Based on these results, the effect of the mean flow and of the turbulent fluctuations in TG dynamos are discussed.

Contents

1. Introduction	2
2. Dynamical runs	3
3. Kinematic runs	4
4. Results	5
5. Discussion	9
Acknowledgments	10
References	10

1. Introduction

The magnetic field of planets and stars is believed to be the result of a dynamo instability originating in the motions inside their electrically conducting fluid core. A dynamo occurs when induction due to motion overcomes diffusion [1], corresponding to a threshold in the magnetic Reynolds number ($R_M = UL/\eta$, with U and L characteristic velocity and length scales of the flow, and η the magnetic diffusivity). For liquid metals (such as molten iron in the Earth core, or liquid sodium in laboratory experiments [2]), the kinematic viscosity $\nu \ll \eta$, and the magnetic Prandtl number $P_M = \nu/\eta$ is $\sim 10^{-5}$ or lower. Thus, the Reynolds number $R_V = UL/\nu = R_M/P_M$ of dynamo generating flows tends to be very high: critical values R_M^c of the order of a few tens are associated with Reynolds numbers in excess of one million.

Here, following the practice in laboratory experiments (and also in several astrophysical and geophysical flows), we focus on flows generated by a deterministic forcing at large-scales. For these, a mean flow develops in addition to turbulent fluctuations which (as observations show) are present in all spatial and temporal scales with correlation length and times extending to the integral scale. In a previous work [3] we considered the flow generated by Taylor–Green (TG) forcing at large-scales. Lowering P_M to 10^{-2} , we established that the value of the threshold for dynamo action R_M^c , of the order of 20 for the laminar flow at low R_V , undergoes an eightfold increase as unsteadiness and small-scale motions develop. It was also observed that once turbulence is fully established, R_M^c saturates to a constant value. For planetary bodies or laboratory experiments, the numerical prediction of the dynamo threshold in realistic conditions is still out of reach. Nonetheless, the experiments [4] in Riga and Karlsruhe found the onset to be remarkably close to the values predicted from kinematic dynamo simulations based on the mean flow structure [5]. However, the flows in these experiments were heavily constrained to reproduce the main characteristics of the Ponomarenko and G O Roberts flows respectively.

These results have led several experimental groups seeking dynamo action in less constrained geometry (eventually leading to richer dynamical regimes) to optimize the mechanical forcing using kinematic simulations based on mean flow measurements [6, 7]—with the advantage that mean flow profiles can be measured in the laboratory. It is thus of interest to test the validity of this procedure, and possibly to clarify the role played in magnetic field amplification by the mean flow as well as by the turbulent fluctuations.

We compare here numerically the dynamo behaviour as simulated from the magneto-hydrodynamics (MHD) equations (1) and (2), to the result of kinematic calculations in which the velocity is fixed to its time-averaged profile. In the fully dynamical problem, we integrate pseudospectrally the following equations in a 2π -periodic box:

$$\frac{\partial \mathbf{v}}{\partial t} + \mathbf{v} \cdot \nabla \mathbf{v} = -\nabla \mathcal{P} + \mathbf{j} \times \mathbf{B} + \nu \nabla^2 \mathbf{v} + \mathbf{F}, \quad (1)$$

$$\frac{\partial \mathbf{B}}{\partial t} + \mathbf{v} \cdot \nabla \mathbf{B} = \mathbf{B} \cdot \nabla \mathbf{v} + \eta \nabla^2 \mathbf{B}, \quad (2)$$

together with $\nabla \cdot \mathbf{v} = \nabla \cdot \mathbf{B} = 0$; a constant mass density $\rho = 1$ is assumed. Here, \mathbf{v} stands for the velocity field, \mathbf{B} is the magnetic field (or the Alfvén velocity), $\mathbf{j} = (\nabla \times \mathbf{B})/\mu_0$ is the current

density, and \mathcal{P} is the pressure. The forcing term \mathbf{F} is given by the TG vortex [8]

$$\mathbf{F}_{\text{TG}}(k_0) = 2F \begin{bmatrix} \sin(k_0x) \cos(k_0y) \cos(k_0z) \\ -\cos(k_0x) \sin(k_0y) \cos(k_0z) \\ 0 \end{bmatrix}, \quad (3)$$

with $k_0 = 1$. In [3] $k_0 = 2$ was used and thus, at the same resolution, the Reynolds numbers, based on the energy containing scale, are here approximately twice that of the previous study.

For a given viscosity, we first let the flow settle into a statistically hydrodynamic (non-magnetic) steady state (only equation (1) is solved with $\mathbf{B} = \mathbf{0}$). We either use direct numerical simulations (DNS) for flows with R_V up to ~ 1000 and P_M down to ~ 0.2 , or large eddy simulation (LES) schemes with an effective viscosity ν_{eff} [9] for P_M lower than about 0.01. Details of the dynamical runs are given in section 2. In the kinematic runs, equation (2) alone is solved with a prescribed (average) flow, details are given in section 3. Section 4 presents the results of both sets of simulations, and compares the values of R_M^c for each set. Finally, section 5 contains some conclusions and discusses the implications of these results for our understanding of large- and small-scale dynamo action when $P_M < 1$ and a large-scales flow is present in the system.

2. Dynamical runs

We first describe our dynamical runs. The mechanical Reynolds number is increased by lowering ν and keeping $F = 1.5$ fixed; numerical grid sizes go from 64^3 to 256^3 . For all runs, the ratio of the largest resolved wavenumber k_{max} to the viscous dissipation one k_ν is larger than one, ensuring a correct hydrodynamic resolution [10]. Moreover, we computed structure functions in DNS $S_p(\mathbf{l}) = \langle [\mathbf{v}(\mathbf{x}) - \mathbf{v}(\mathbf{x} + \mathbf{l})]^p \rangle$ up to order $p = 4$. As is conventional in numerical simulations of turbulence we have verified that at small-scales the velocity increments obey the trivial scaling $S_p(l) \sim l^p$ for $\ell_{\text{min}} < |\mathbf{l}| < 3\ell_{\text{min}}$ where $\ell_{\text{min}} = 2\pi/k_{\text{max}}$ is the smallest increment in physical space [31]. Thus the small-scales field is smooth and the dissipation is well captured in the DNS.

Once the hydrodynamic steady state is reached, a seed magnetic field with energy 10^{-20} evenly distributed among Fourier modes is introduced, and the MHD equations are integrated for several magnetic diffusion times. For each run, we compute the growth rate $\sigma_B = d(\ln E_M)/dt$, where E_M is the magnetic energy. The critical magnetic Reynolds number in the dynamical runs, denoted as $R_{M,\text{dyn}}^c$, is defined as the value of R_M for which σ_B changes sign at fixed R_V . In these runs, $R_{M,\text{dyn}}$ is defined as $R_{M,\text{dyn}} = U_{\text{dyn}} L_{\text{dyn}}/\eta$ where U_{dyn} and L_{dyn} are respectively the r.m.s. velocity and integral scale in the dynamical flow before the magnetic seed is introduced—a precise definition of the integral scale is given below in equation (5). In the DNS, equations (1) and (2) are numerically integrated, whereas in the LES the large-scales dynamic is accounted for but the velocity fluctuations at scales smaller than the Ohmic dissipation scale are modelled (as a result, the magnetic field is directly resolved at all scales) [3, 9, 11]. The LES was validated against experiments in [9], and the value of R_M^c from the LES was validated against DNS and another subgrid model of MHD turbulence in [3].

Table 1. Run parameters for cases where the mean flow is computed: grid resolution, viscosity (effective value for the last run with LES), integral length and velocity scales, Reynolds number $R_{V,\text{dyn}} = L_{\text{dyn}}U_{\text{dyn}}/\nu$, critical magnetic Reynolds number $R_{M,\text{dyn}}^c$ for the dynamical problem and for the kinematic ones ($R_{M,\text{kin}}^{c1}$ at onset of the first dynamo mode, $R_{M,\text{kin}}^{c2}$ when it no longer grows, and $R_{M,\text{kin}}^{c3}$, the onset of the second dynamo mode). The $R_{M,\text{kin}}$ values are computed using the kinematic integral velocity and length scales, and the critical magnetic diffusivity: $R_{M,\text{kin}}^{ci} = L_{\text{kin}}U_{\text{kin}}/\eta^{ci}$, where $i = 1, 2$ or 3 . The asterisk indicates the run is an LES.

N	ν	L_{dyn}	U_{dyn}	$R_{V,\text{dyn}}$	$R_{M,\text{dyn}}^c$	$R_{M,\text{kin}}^{c1}$	$R_{M,\text{kin}}^{c2}$	$R_{M,\text{kin}}^{c3}$
64	0.3	3.1	1.4	15	34	22.0	53.2	142
64	0.1	3.3	2.2	77	48	23.9	48.7	150
64	0.08	3.5	2.3	98	59	23.7	50.6	155
128	0.04	3.4	2.5	190	110	23.3	51.6	152
128	0.015	2.6	2.6	460	170	24.6	50.8	149
256	0.007	2.4	2.8	930	180	22.3	52.6	145
128*	8.6×10^{-4}	2.3	2.8	7950	150	23.5	51.2	167

3. Kinematic runs

Kinematic runs (cf table 1) are later computed for a subset of the dynamical runs, for which we define the mean flow \mathbf{U} as a time average of the dynamical velocity \mathbf{v} :

$$\mathbf{U}(\mathbf{r}) = \frac{1}{T} \int dt \mathbf{v}(\mathbf{r}, t), \quad (4)$$

where T is a time much larger than an eddy turnover time T_{NL} at the integral scale L_{dyn} , i.e. $T \ll T_{\text{NL}} = U_{\text{dyn}}/L_{\text{dyn}}$. Note that T should exceed the magnetic diffusion time $T_{\text{M}} = R_{\text{M}}T_{\text{NL}}$. In practice, an instantaneous velocity field is extracted from the dynamical simulations every time interval ΔT to increment the running average of $\mathbf{U}(\mathbf{r})$. We used $\Delta T \sim T_{\text{NL}}/100$, and $T > 200T_{\text{NL}}$. To save computer time, the averaging is done during the linear growth (or decay) phase in the dynamical runs—hence in the absence of a Lorentz feedback in the Navier–Stokes equation. Equation (2) is then solved with $\mathbf{v}(\mathbf{r}, t) \equiv \mathbf{U}(\mathbf{r})$, in search of growing solutions $E_{\text{M}}(t) = E_{\text{M}}^0 \exp(\sigma_{\text{B}}^{\text{kin}} t)$ with positive $\sigma_{\text{B}}^{\text{kin}}$. Note that the mean flow (see equation (4)) is no longer a solution of the hydrodynamic equations. For instance, it does not have a well-defined viscosity in the sense that there is no known relationship from which one could compute a viscosity from the $\mathbf{U}(\mathbf{r})$ as opposed to the dynamical flow for which the velocity skewness is related to the dissipation and, hence, the viscosity. We therefore chose to attribute to the mean flow the viscosity of its generating dynamical run. Then one can also define an associated kinematic Reynolds number $R_{V,\text{kin}} = U_{\text{kin}}L_{\text{kin}}/\nu$, but instead we chose to represent all mechanical Reynolds number variations as a function of $R_{\text{V}} \equiv R_{V,\text{dyn}}$ (see e.g. figures 1 and 3).

As for the magnetic Reynolds numbers, two definitions can be introduced. The critical magnetic Reynolds number can be given in terms of $R_{M,\text{dyn}}$ or $R_{M,\text{kin}}$, computed from each field’s characteristic lengths and r.m.s. velocities. Instead of giving two critical values for all kinematic runs, figure 2 shows the thresholds R_{M}^c for the kinematic runs in units of $R_{M,\text{kin}}$ (see also

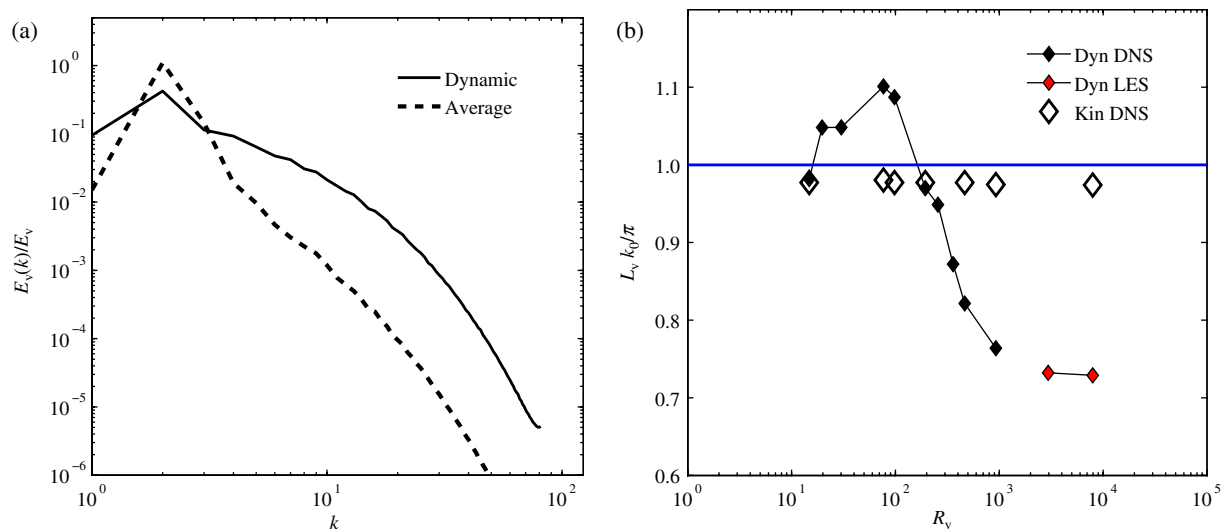


Figure 1. (a) Kinetic energy spectra for TG1 ($\nu = 0.007$); dynamical spectrum $E_{V,\text{dyn}}(k, t = T)$ (solid line), and average flow spectrum $E_{V,\text{kin}}(k)$ (dotted line); (b) integral length scales L_{dyn} and L_{kin} , normalized by the size of the unit TG cell, versus the flow Reynolds numbers $R_V \equiv R_{V,\text{dyn}}$.

table 1), and two curves corresponding to the thresholds for the dynamical runs in units of $R_{M,\text{dyn}}$ and $R_{M,\text{kin}}$.

4. Results

Before analysing the dynamo behaviour, we first compare characteristics of the dynamic and time-averaged velocity fields. Their spectra are shown in figure 1(a), for the DNS calculation at $R_{V,\text{dyn}} \approx 930$. While the dynamical flow has a typical turbulence spectrum, the time-averaged field is sharply peaked at the size of the TG cell. As the mechanical Reynolds number varies the properties of the average flow are the same, while they do vary for the dynamical field. For instance, the flow integral scale computed from the kinetic energy spectrum as

$$\frac{L}{2\pi} = \left\langle \frac{\int dk E_V(k, t)/k}{\int dk E_V(k, t)} \right\rangle_T \quad (5)$$

is shown in figure 1(b); we define $\langle \cdot \rangle_T$ as a time average and we recall that the TG flow is forced at $k_0 = 1$. For mechanical Reynolds numbers smaller than about 100, L_{dyn} tends to be larger than the size of one TG vortex ($\approx \pi$). At higher R_V s, the turbulent flow has an integral lengthscale clearly confined within the TG cell. The mean flow, however, has $L_{\text{kin}} \approx \pi$ and $U_{\text{kin}} \approx 3$ at all R_V s.

We now turn to the dynamo generation. In the dynamical problem, the $R_{M,\text{dyn}}^c$ versus R_V curve—figure 2(b)—displays an initial increase, corresponding to the development of turbulence, followed by a plateau [3] where the threshold is independent of viscosity. This behaviour has been observed now for several coherent forcing functions (helical and non-helical) [3, 12, 13], while for isotropic and homogeneous random forcing no saturation of $R_{M,\text{dyn}}^c$ as a function of R_V

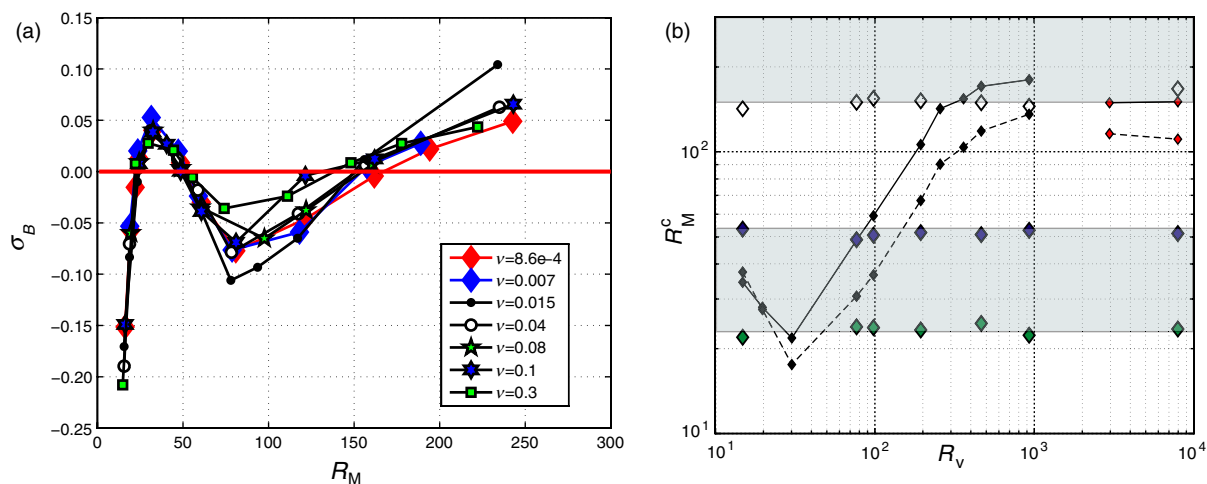


Figure 2. (a) Growth rates for the kinematic dynamo generated by mean flows computed for decreasing viscosity. Crossing the $\sigma_B = 0$ axis defines the $R_{M,\text{kin}}^{1,2,3}$ values reported in table 1. (b) Evolution of the critical magnetic Reynolds numbers $R_{M,\text{kin}}^c$ and $R_{M,\text{dyn}}^c$ with R_V . Symbols: the green, blue and white parallelograms mark the dynamo windows for the kinematic low and high modes; the smaller symbols follow the dynamical curves (black: DNS, red: LES) plotted either in units of $R_{M,\text{dyn}}$ (solid line) or in units of $R_{M,\text{kin}}$ (dashed line)—see text for further details. The shaded areas indicate regions of dynamo action as obtained from the time-average runs, in units of $R_{M,\text{kin}}$. The dynamical run at $R_V = 928$ is a 256^3 DNS computation, higher Reynolds number are reached using LES). Note that the lowest P_M for a dynamo is 10^{-2} .

has been found so far (see e.g. [14, 30] and references therein). In the case of coherent forcing, both excitation of magnetic field lines at scales smaller than the forcing scale (with all Fourier modes growing with the same growth rate), and excitations of large-scales magnetic fields (which keep growing after the small-scales saturate) are observed [12]. This suggests that the mean flow associated with the coherent forcing plays an important role to obtain an asymptotic behaviour of R_M^c for $P_M < 1$. However, the effect of the turbulent fluctuations on the value of R_M^c and dynamo action is harder to elucidate and to separate from the effect of the mean flow.

For kinematic simulations using the time-averaged flow, we found the existence of two distinct dynamo branches—a behaviour already revealed in the *ABC* flow [15]. As shown in figure 2(a), the kinematic growth rate is positive in the interval $[R_{M,\text{kin}}^1, R_{M,\text{kin}}^2] \approx [22, 50]$, and then again for $R_{M,\text{kin}} > R_{M,\text{kin}}^3 \approx 160$. Beyond $R_{M,\text{kin}}^3$ the growth rate seems to be monotonously increasing with R_M . We call the interval $[R_{M,\text{kin}}^1, R_{M,\text{kin}}^2]$ the ‘first dynamo window’ (the corresponding interval is shaded in figure 2(b)). We observe this window is essentially independent of the mechanical Reynolds number $R_{V,\text{dyn}}$ from which the time-averaged flow is generated. The threshold for the upper dynamo branch— $R_{M,\text{kin}}^3$ —also appears to be independent of the kinetic Reynolds number; we have observed that it remains within 15% of the value $\langle R_{M,\text{kin}}^3 \rangle \approx 160$ when R_V is varied across our explored range $[10, 10^4]$.

Essential findings in this paper come from the comparison of the above kinematic behaviour with the results obtained for the dynamo thresholds computed for the dynamical fields. The data

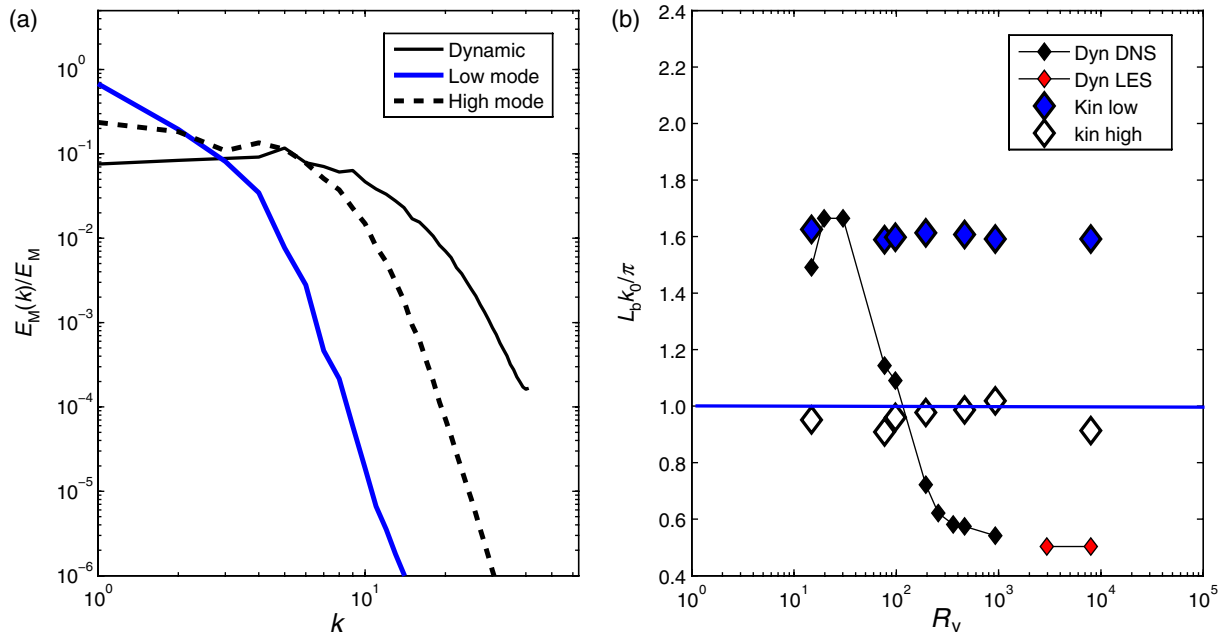


Figure 3. (a) Magnetic energy spectra for $\nu = 0.007$; (solid line) dynamical run, (thick blue solid line) low and (short dashed lines) high R_M kinematic dynamo modes in the average flow—in this regime the spectra are computed as averages during the growth phase, normalized by the mean energy. (b) Evolution of the integral scales for the magnetic field, computed from the spectra.

are shown in figure 2(b) in which all critical magnetic Reynolds numbers R_M^c are plotted against the kinetic Reynolds number R_V . At low R_V , the dynamo threshold for the dynamical runs $R_{M,dyn}^c$ lies within first dynamo window of the time-averaged flow. But as R_V exceeds about 200, $R_{M,dyn}^c$ is found in the immediate vicinity of the upper dynamo branch of the time-averaged flow.

A quite noteworthy feature is revealed when the dynamo thresholds obtained for the dynamical fields are plotted in terms of $R_{M,kin}^c$, i.e. using L_{kin} and U_{kin} as length and velocity scales [16]. Then one observes that dynamo action takes place outside the windows for which kinematic dynamos are found. Actually, the threshold computed in this way is below the kinematic upper branch. We attribute this difference as evidence of the role of turbulent fluctuations. At this point it may be unclear from figure 2(b) whether the effect of the fluctuations in the dynamical runs is to increase the threshold from the first kinematic window, or to decrease the threshold from the second kinematic branch. We shall return to this issue in the discussion section.

A comparison of the structure of the resulting dynamo fields, the magnetic energies, and the corresponding integral length scales is shown in figure 3. For the dynamical dynamo runs, energy is distributed in a broad range of scales. For the kinematic dynamos evolved from the time-averaged flow, we observe that for the low R_M mode the energy is strongly peaked at large-scales, while it is more evenly distributed in the case of the high R_M mode. However, the magnetic energy spectrum is not as broad as in the dynamical runs using the instantaneous flow. Note also the dynamical runs have a range of wavenumbers (at the large-scales) where the slope of the magnetic energy spectrum is positive, while the spectrum in the kinematic runs monotonically decreases with increasing wavenumber. This difference can be the result of the lack of dynamo action from the large- and small-scale fluctuations in the runs done using the average flow.

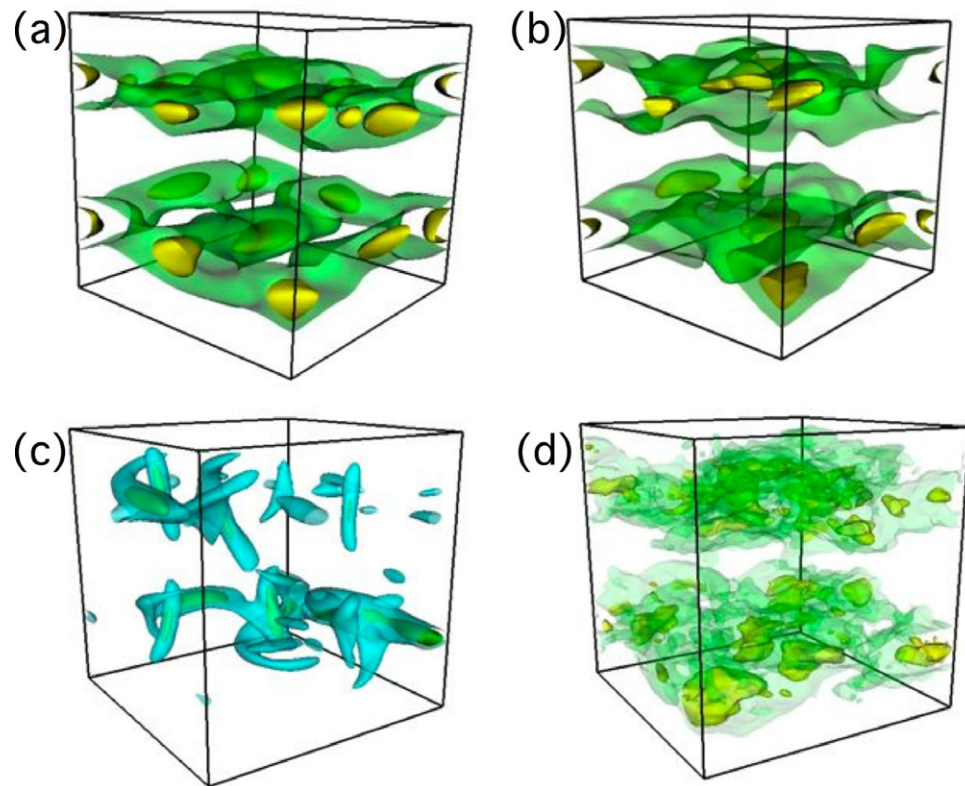


Figure 4. Isosurfaces of the magnetic energy. (a) TG1 kinematic low eigenmode; (b) corresponding dynamical run at $R_V = 76.74$; (c) high kinematic eigenmode; (d) corresponding dynamical run at $R_V = 465$. Isovalues at 50 and 75% of the maximum of E_M for (a) and (b) and 25 and 50% for (b) and (d).

Changes in dynamo behaviour are also reflected in the evolution of the magnetic integral scale L_B , shown in figure 3(b). The kinematic ‘low mode’ grows a dynamo essentially at scales *larger* than the TG cell ($L_B \approx 1.6\pi$) at all R_V . For the ‘high mode’ on the other hand, magnetic fields grow within a TG vortex. The dynamo mode selected by the dynamical flow seems to switch between these two behaviours. At low R_V it grows with an integral scale larger than the TG cell, and we observe that $L_{B,\text{dyn}} \sim L_{B,\text{kin}}$. At high R_V the magnetic integral scale is about half the size of the TG cell. The peak in the magnetic energy spectrum at smaller scales in the dynamical runs, as well as the smaller integral scale, together with the differences in the two dynamical curves in figure 2(a), suggest that turbulent fluctuations may play a role enhancing the dynamo—in agreement with [12] where both large- and small-scales were observed to cooperate. The growth of small magnetic scales allows the quenching of velocity fluctuations later in the nonlinear regime, and hence helps the growth of the magnetic field at large-scales.

The structure of the dynamos can be explored further with visualizations of isosurfaces of magnetic energy in real space. Figures 4(a) and (c) correspond respectively to the low and high kinematic dynamo modes, while figures 4 (b) and (d) show the dynamical fields, with the magnetic energy rescaled and averaged in time during the linear growth phase (i.e. $\langle E_M(\mathbf{x}, t) / E_M(t) \rangle_T$) for $R_V \approx 77$ and $R_V \approx 460$. One observes a good correspondence between the low R_V dynamical mode and the kinematic low eigenfunction; indeed, at low Reynolds number the flow is laminar

with small fluctuations about its mean; in this regime the dynamo is mainly generated in the shearing regions between the TG cells [12, 17]. At high R_V , comparing the dynamical growing dynamo to the structure of the high R_M eigenfunction, we recognize in figure 4(c) the ‘twisted banana’ structure of the neutral mode that underlies the $\alpha - \Omega$ dynamo in von Kármán flows (note that at high R_V the TG flow in each cell is similar to the von Kármán swirling flow) [7, 17]. For the dynamical flow at high R_V the TG cells are no longer as coupled as they are at low R_V , and in figure 4(d) one does not observe the clear pattern of the kinematic eigenmode. As seen in the spectrum—figure 3(a)—the magnetic energy in the dynamical runs at high R_V grows at all scales; it is only in the nonlinear phase that the magnetic energy is eventually dominated by the large-scales. However, at all R_V s the dynamo grows predominantly in the planes $\pi/2$ and $3\pi/2$ which cut through the centre of the TG cells. We observed a similar behaviour for TG flows forced at $k_0 = 2$ (two branches in the kinematic dynamo problem, and a transition of the value of R_M^c in the dynamical runs from the lower kinematic runs to a value close to the higher branch as turbulence develops). Results may differ for other types of forcings [13].

5. Discussion

The observations made, particularly at large R_V , may have some relevance for laboratory experiments. For instance, we find that once turbulence is fully developed, the dynamo threshold in the dynamical runs (in units of $R_{M,dyn}^c$) is well approximated by the (high branch) kinematic value $R_{M,kin}^c$ computed using the time-averaged flow. Differences between the threshold in the dynamical runs in units of $R_{M,kin}^c$ and $R_{M,dyn}^c$ can be attributed to the effect of turbulent fluctuations, as is discussed below. These findings are in agreement with the observations in the Riga and Karlsruhe experiments, where the mean flow structure was optimized to favour dynamo action with a moderate value of R_M^c ; it agrees as well with analytical predictions for small amplitude fluctuations around the mean flow structure [18].

We also observe that the threshold reaches an asymptotic value when R_V grows, in agreement with kinematic simulations using von Kármán mean flows measured in the laboratory [7]: the threshold was observed to be R_V independent for R_V in excess of $\sim 10^5$. Hence one may expect that kinematic predictions based on hydrodynamic measurements in laboratory prototypes can be useful for experiments. This is also of interest for numerical studies of natural dynamos, where a fully resolved description of the fluid motions in the correct range of parameters is currently out of reach [19]. There are however reasons to be cautious. The main concern lies in the observation that fully turbulent flows in confined volumes are not stationary: long-time dependence (i.e. slow changes) in the large-scales velocity fluctuations has been observed [20, 21]. Also, the effect of turbulent fluctuations on the threshold may need further study. While recent works have shown that a large-scales incoherent noise may increase significantly the dynamo threshold [22], small-scale fluctuations can also be a source of dynamo action [1, 23, 24].

This leads us to our last question. The central role played by the average flow is clear from the kinematic simulations. But can the results obtained so far be used to elucidate the role played by the velocity fluctuations in the dynamo process when $P_M < 1$ and a mean flow is present? Two scenarios can be foreseen. The net effect of velocity fluctuations can be to enhance the magnetic effective diffusivity (thus giving a larger value of R_M^c in the dynamical runs than in the kinematic runs), or to be a source of dynamo action (thus giving a smaller value of R_M^c). Analysis of kinematic runs perturbing the average flow with synthetic noise seem to suggest

the first scenario [22], but it should be remarked that the properties of the turbulent fluctuations are not independent of the properties of the flow in the large-scales [25]. On the other hand, the results presented here and results from spectral transfer analysis [26] seem to favour the second scenario.

Let us review the evidence so far. The analysis presented here separates mean flow from fluctuations based on timescales. This is a common practice in studies of turbulent flows, that can be complemented by a separation based on lengthscales. From the timescale analysis, we observe that the value of R_M^c in the dynamical runs is smaller than the corresponding value of the ‘high branch’ in the kinematic runs when both quantities are plotted in units of $R_{M,kin}^c$ (see figure 2). However, the dynamical dynamo mode shares some properties with the ‘high branch’ kinematic mode. We also observe a positive slope in the magnetic energy spectrum ($\sim k^{3/2}$ [3]) of the dynamical runs that is not observed in the kinematic average-flow simulations. This positive slope is consistent with (non-local) dynamo contributions [23, 24], [27]–[29] due to the turbulent fluctuations (possible in the large-scales) and certainly not with a direct magnetic energy transfer.

A spectral analysis based on lengthscales [26] also showed that turbulent fluctuations at all scales give nonlocal stretching of magnetic field lines. For TG forcing (at $k_0 = 2$), $R_M \approx 680$ and $P_M < 1$ it was found that the fluctuations at all wavenumbers up to $k \approx 12$ are also a source of dynamo action that overcomes Ohmic diffusion as well as the removal of magnetic energy due to the direct transfer to smaller scales (a turbulent enhanced diffusion), thus contributing to the positive growth rate in all these wavenumbers. The observations presented, both in the time and space domain, indicate fluctuations at all scales (even at the forced scales) play a role in magnetic field amplification, and that under the proper conditions (e.g. if the mechanical and magnetic Reynolds numbers are large enough) the dynamo action due to these fluctuations can overcome the enhanced turbulent dissipation and cooperate with the stretching of magnetic field lines due to the average flow.

Acknowledgments

We thank F Daviaud, B Dubrulle, R Volk and A Schekochihin for useful discussions. PDM and AP acknowledge partial support from NSF CMG–0327888 at NCAR. JFP, HP and YP thank CNRS Dynamo GdR, INSU/PNST, and PCMI Programs. Computer time was provided by NCAR, PSC, NERSC, IDRIS and the Mesocentre SIGAMM machine, hosted by Observatoire de la Cote d’Azur.

References

- [1] Moffatt H K 1978 *Magnetic Field Generation in Electrically Conducting Fluids* (Cambridge: Cambridge University Press)
- [2] 2002 Special issue: MHD dynamo experiments *Magnetohydrodynamics* **38**
- [3] Ponty Y, Minnini P D, Pouquet A, Politano H, Montgomery D C and Pinton J-F 2005 *Phys. Rev. Lett.* **94** 164512
- [4] Steiglitz R and Müller U 2001 *Phys. Fluids* **13** 561
Gailitis A et al 2000 *Phys. Rev. Lett.* **84** 4365
- [5] Gailitis A 1996 *Magnetohydrodynamics* **1** 63
Tilgner A 1997 *Phys. Rev. A* **226** 75
- [6] Bayliss R A, Forest C B, Nornberg M D, Spence E J and Terry P W 2007 *Phys. Rev. E* at press

- [7] Marié L, Burguete J, Daviaud J and Léorat J 2003 *Eur. J. Phys. B* **33** 469
Ravelet F *et al* 2005 *Phys. Fluids* **17** 117104
- [8] Brachet M 1990 *C. R. Acad. Sci. Paris* **311** 775
Brachet M 1991 *Fluid Dyn. Res.* **8** 1
- [9] Ponty Y, Politano H and Pinton J-F 2004 *Phys. Rev. Lett.* **92** 144503
- [10] Kaneda Y *et al* 2003 *Phys. Fluids* **15** L21
Yoshida K, Ishihara T and Kaneda Y 2003 *Phys. Fluids* **15** 2385
- [11] Knaepen B and Moin P 2004 *Phys. Fluids* **16** 1255
- [12] Mininni P D, Ponty Y, Montgomery D C, Pinton J-F, Politano H and Pouquet A 2005 *Astrophys. J.* **626** 853
- [13] Mininni P D and Montgomery D C 2005 *Phys. Rev. E* **72** 056320
- [14] Schekochihin A A, Haugen N E L, Brandenburg A, Cowley S C, Maron J L and McWilliams J C 2005 *Astrophys. J.* **625** L115
- [15] Galloway D J and Frisch U 1986 *Geophys. Astrophys. Fluid Dyn.* **36** 53
- [16] Ponty Y, Mininni P D, Pinton J-F, Politano H and Pouquet A 2006 *Preprint physics/0601105*
- [17] Nore C, Brachet M, Politano H and Pouquet A 1997 *Phys. Plasmas* **4** 1
- [18] Pétrélis F and Fauve S 2001 *Eur. Phys. J. B* **22** 273
- [19] Dormy E, Valet J-P and Courtillot V 2000 *Geochem. Geophys. Geosyst.* **1** 62
- [20] Bourgoin M, Marié L, Petrelis F, Burguete J, Chiffaudel A, Daviaud F, Fauve S, Odier P and Pinton J-F 2001 *Phys. Fluids* **14** 3046
- [21] Volk R, Odier P and Pinton J-F 2006 Fluctuation of magnetic induction in von Kármán swirling flows *Phys. Fluids* **18** 085105
- [22] Laval J-P, Blaineau P, Leprovost N, Dubrulle B and Daviaud F 2005 *Phys. Rev. Lett.* **96** 204503
- [23] Zeldovich Ya, Ruzmaikin A and Sokoloff D 1983 *Magnetic Fields in Astrophysics* (New York: Gordon and Breach)
- [24] Kraichnan R H 1968 *Phys. Fluids* **11** 945
Kazantsev A P 1968 *Sov. Phys.—JETP* **26** 1031
- [25] Alexakis A, Mininni P D and Pouquet A 2005 *Phys. Rev. Lett.* **95** 264503
Mininni P D, Alexakis A and Pouquet A 2006 *Phys. Rev. E* **74** 016303
Poulain C, Mazellier N, Chevillard L, Gagne Y and Baudet C 2006 *Eur. Phys. J. B* **53** 219
- [26] Alexakis A, Mininni P D and Pouquet A 2005 *Phys. Rev. E* **72** 046301
Mininni P D, Alexakis A and Pouquet A 2005 *Phys. Rev. E* **72** 046302
- [27] Schekochihin A A, Cowley S C, Taylor S F, Maron J L and McWilliams J C 2004 *Astrophys. J.* **612** 276
- [28] Vainshtein S and Kichatinov L 1986 *J. Fluid Mech.* **168** 73
Boldyrev S and Cattaneo F 2004 *Phys. Rev. Lett.* **92** 144501
- [29] Haugen N E L, Brandenburg A and Dobler W 2004 *Astrophys. Space Sci.* **292** 53
- [30] Schekochihin A A, Cowley S, Hammett G, Maron J and McWilliams J C 2002 *New J. Phys.* **4** 84
Schekochihin A A, Cowley S, Maron J and McWilliams J C 2004 *Phys. Rev. Lett.* **92** 054502
- [31] Davidson P 2000 *Turbulence* (Oxford: Oxford University Press)